ELSEVIER

International Journal of Solids and Structures 41 (2004) 3211–3224

INTERNATIONAL JOURNAL OF SOLIDS and STRUCTURES

www.elsevier.com/locate/ijsolstr

Dynamic compressive strengths of polymeric composites

Jialin Tsai [1], C.T. Sun *

School of Aeronautics and Astronautics, Purdue University, 325 N. Grant Street, West Lafayette, IN 47907-1282, USA

Received 8 May 2003; received in revised form 14 November 2003

Available online 13 February 2004

Abstract

The dynamic compressive strength of unidirectional fiber composites in the form of fiber microbuckling was investigated and modeled. Both strain rate and shear stress effects on the compressive strength were considered. The present model was developed from extending Rosen's fiber buckling model in conjunction with a viscoplasticity model to describe the inelastic and rate dependent behavior of the composite. Off-axis S2/8552 glass/epoxy composite specimens were tested at various strain rates to provide the experimental data with the presence of shear stresses. For strain rates below 1 s^{-1}, compression tests were conducted on an MTS loading machine, while higher strain rate tests were performed using a split Hopkinson pressure bar (SHPB). Comparison of model predictions with experimental data showed that the dynamic microbuckling model was quite accurate in predicting compressive failure of unidirectional composites for strain rates up to 900 s^{-1}. From the model predictions and experimental data, it was found that the presence of shear stress can significantly lower the compressive strength of composites. Comparison of the present microbuckling model and the kink band model was made.

Keywords: Polymeric composites; Compressive strength; Strain rate; Shear stress; Microbuckling; Split; Hopkinson pressure bar

1. Introduction

For most materials, the compressive strength is much greater than the tensile strength. Fiber-reinforced composites are among the very few materials that exhibit a greater tensile strength than compressive strength. This behavior results from that the compressive failure mechanism in fiber composites is in the form of fiber microbuckling. Static compressive strengths of unidirectional composites have been studied by many researchers in past few decades. Two main models have been developed for predicting compressive strengths of fiber composites, namely, the microbuckling model and the kink band model. In the microbuckling model, the compressive failure was assumed to be triggered by the local instability of fibers embedded in the matrix as depicted in Fig. 1. Rosen (1965) was the first researcher to propose a fiber

* Corresponding author. Tel.: +1-765-4945130; fax: +1-765-4940307.
E-mail address: sun@ecn.purdue.edu (C.T. Sun).
[1] Currently, Assistant Professor, Department of Mechanical Engineering, National Chiao Tung University, Hsinchu, Taiwan.

0020-7683/$ - see front matter © 2003 Elsevier Ltd. All rights reserved.
doi:10.1016/j.ijsolstr.2003.12.010

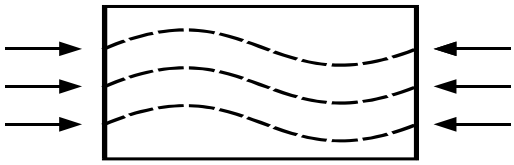

Fig. 1. Shear mode microbuckling model.

microbuckling model based on perfectly aligned elastic fibers and elastic matrices. However, the predicted compressive strength according to this model was much higher than the experimental data. Sun and Jun (1994) followed Rosen's concept and developed a microbuckling model that included the effects of fiber misalignments and the nonlinear behavior of the matrix with an improved accuracy in prediction.

On the other hand, the kink band model (see Fig. 2) was developed with the assumption that compressive failure of the composite results from yielding of shear deformation in the composite in connection with initially misaligned fibers. Argon (1972) investigated the fiber misalignment effect on compressive failure and suggested that, once the shear stress in the region of fiber misalignments reached the composite shear yield stress, compressive failure would occur. In his model, the composite material was assumed to be rigid plastic. Budiansky (1983) and Budiansky and Fleck (1993) extended Argon's model to include more general elastic–plastic behavior of composites.

In either the microbuckling model or the kink band model, the compressive strength of a fiber composite is governed by the matrix stiffness property. Thus, it is reasonable to expect a pronounced strain rate effect. Many researchers have investigated the dynamic compressive behavior in composites. Kumar et al. (1986) performed dynamic compressive tests on glass/epoxy composites for various fiber orientations. The dynamic compressive strength for the 0° specimen was found to have increased nearly 100% compared with the static value, and the failure was dominated by fiber splitting. For off-axis specimens with fiber orientations larger than 10°, experimental data indicated that matrix shearing was the main failure mode. El-Habak (1993) studied the strain rate effect on the compressive strength of unidirectional glass/epoxy composites. He found that, in contrast to the results by Kumar et al. (1986), the compressive strength was only slightly increased with strain rate. Lankford (1991) tested a carbon fiber-reinforced thermoplastic matrix composite (AS4/PEEK) in compression at strain rates ranging from 10^{-5} to 5000 s^{-1}. In order to prevent fiber brooming, steel ring fittings were placed at both ends of the cylindrical specimen. The test results showed that, for strain rates less than 1000 s^{-1}, compressive strength increased somewhat as strain rate increased. However, for strain rates on the order of 10^3–10^4 s^{-1}, the compressive strength sharply increased. For strain rates less than 1000 s^{-1}, kinking was found to be the dominant failure mode; while, for strain rates in excess of 1000 s^{-1}, the dominant failure mechanism could not be determined because the specimen was destroyed in the high strain experiment. Yuan et al. (1999) studied the influence of strain rate on compressive strength of glass and carbon fiber-reinforced unidirectional composites with different fiber volume fractions. It was found that kinking followed by longitudinal splitting was the main failure mechanism, and that compressive strength was dependent on strain rate.

So far, theoretical models for predicting compressive strengths of fiber composites at high strain rates are still lacking. The purpose of this study was to develop a theoretical model that is capable of predicting

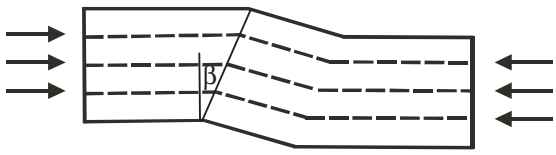

Fig. 2. Kink band model.

compressive strengths of polymeric fiber composites under both static and dynamic loads. The microbuckling model was established with off-axis compression tests together with the aid of a viscoplasticity model for composites. Off-axis specimens with small off-axis angles were tested using a split Hopkinson bar to verify the model predictions at high strain rates.

2. Microbuckling model

Rosen (1965) employed a 2-D elasticity model to estimate the buckling condition of fibers in a composite. The buckling stress of the dominant shear mode as shown in Fig. 1 is given by

$$\sigma_{11c} = \frac{G_m}{1 - c_f} \tag{1}$$

where G_m and c_f are matrix shear modulus and fiber volume fraction, respectively. The compressive strength predicted based on Rosen's elastic microbuckling model was found to be much greater than the experimental results. It was suggested that the discrepancy could be attributed to the misalignment of fibers and the nonlinear behavior of the matrix.

Fiber misalignment is a manufacturing defect created by fiber movements in the matrix during the lay-up and curing processes. As a result of the presence of fiber misalignments, shear stresses in the matrix may be produced when the composite is subjected to nominally axial compressions. These shear stresses can lead to early onset of yielding of the matrix, reducing its support to the fiber and resulting in fiber microbuckling. Thus, shear stresses induced by fiber misalignments can influence the compressive strength of a fiber composite. Sun and Jun (1994) extended the microbuckling model by taking into account the effects of fiber misalignment and matrix nonlinearity and obtained the compressive strength of the composite as

$$\sigma_{11c} = \frac{G_m^{ep}}{1 - c_f} \tag{2}$$

where G_m^{ep} is the elastic–plastic tangent shear modulus of the matrix. It is noted that the elastic–plastic tangent shear modulus G_m^{ep} is not a constant but is dependent on the instantaneous state of stress in the matrix. Based on the 2-D model used by Rosen (1965) and Sun and Jun (1994), in which the composite is represented by an equivalent plate/matrix periodically layered medium, the right-hand side of Eq. (2) is recognized as the elastic–plastic tangent modulus of the composite. Thus, the compressive strength of the composite can be expressed in the form

$$\sigma_{11c} = G_{12}^{ep} \tag{3}$$

where G_{12}^{ep} is the elastic–plastic tangent shear modulus of the composite. Since G_{12}^{ep} depends on the current state of stress in the composite, in general, Eq. (3) must be solved numerically for the compressive strength.

3. Dynamic microbuckling model

Matrix-dominated deformations in polymeric composites are strain rate dependent. Tsai and Sun (2002) investigated the dynamic response of the S2/8552 glass/epoxy composite and found its mechanical behavior to be quite sensitive to strain rate. A viscoplastic constitutive model was developed by Tsai and Sun (2002) for this composite. In the present study, this model is used to derive the strain rate dependent elastic–plastic tangent shear modulus of the composite.

3.1. Derivation of rate dependent tangent shear modulus

For small deformations, the total strain rate can be decomposed into elastic and plastic parts as

$$\dot{\varepsilon}_{ij} = \dot{\varepsilon}^{\mathrm{e}}_{ij} + \dot{\varepsilon}^{\mathrm{p}}_{ij} \tag{4}$$

The one-parameter plastic potential function

$$f = \tfrac{1}{2}\left(\sigma_{22}^2 + 2a_{66}\sigma_{12}^2\right) \tag{5}$$

proposed by Sun and Chen (1989) for modeling static nonlinear behavior of composites is employed to develop the rate dependant viscoplasticity model. In Eq. (5), a_{66} is an orthotropy coefficient, and σ_{ij} are stress components referred to the material principal directions. By using the flow rule, the plastic shear strain rate is expressed as (Tsai and Sun, 2002)

$$\dot{\gamma}^{\mathrm{p}}_{12} = 2a_{66}\sigma_{12}\dot{\lambda} \tag{6}$$

where $\dot{\lambda}$ is a proportionality factor.

Define the effective stress as

$$\bar{\sigma} = \sqrt{3f} = \sqrt{\frac{3}{2}}\left(\sigma_{22}^2 + 2a_{66}\sigma_{12}^2\right)^{1/2} \tag{7}$$

Through the equivalence of plastic work rate

$$\dot{w}^{\mathrm{p}} = \sigma_{ij}\dot{\varepsilon}^{\mathrm{p}}_{ij} = \bar{\sigma}\bar{\dot{\varepsilon}}^{\mathrm{p}} = 2f\dot{\lambda} \tag{8}$$

the effective plastic strain rate $\bar{\dot{\varepsilon}}^{\mathrm{p}}$ is defined and the proportionality factor $\dot{\lambda}$ in Eq. (6) is obtained as (Tsai and Sun, 2002)

$$\dot{\lambda} = \frac{3}{2}\frac{\bar{\dot{\varepsilon}}^{\mathrm{p}}}{\bar{\sigma}} = \frac{3}{2}\frac{\dot{\bar{\sigma}}}{H_{\mathrm{p}}\bar{\sigma}} \tag{9}$$

where

$$H_{\mathrm{p}} = \frac{\dot{\bar{\sigma}}}{\bar{\dot{\varepsilon}}^{\mathrm{p}}} \tag{10}$$

is the rate dependant plastic modulus.

The viscoplasticity model developed by Tsai and Sun (2002) is expressed in the form

$$\bar{\varepsilon}^{\mathrm{p}} = \chi\left(\bar{\dot{\varepsilon}}^{\mathrm{p}}\right)^m(\bar{\sigma})^n \tag{11}$$

where χ, m and n are material constants which can be determined by performing axial compression tests on off-axis specimens at different strain rates. The viscoplasticity model for the S2/8552 composite at high strain rates up to 1000 s^{-1} was verified with the data obtained from the split Hopkinson pressure bar (SHPB) tests conducted by Tsai and Sun (2002).

By using Eq. (11) the plastic modulus defined by Eq. (10) becomes (see Thiruppukuzhi and Sun, 2001)

$$H_{\mathrm{p}} = \frac{\dot{\bar{\sigma}}}{\bar{\dot{\varepsilon}}^{\mathrm{p}}} = \frac{\dot{\bar{\sigma}}\,\mathrm{d}t}{\bar{\dot{\varepsilon}}^{\mathrm{p}}\,\mathrm{d}t} = \frac{\mathrm{d}(\bar{\sigma})}{\mathrm{d}\bar{\varepsilon}^{\mathrm{p}}} = \frac{1}{n\chi\left(\bar{\dot{\varepsilon}}^{\mathrm{p}}\right)^m(\bar{\sigma})^{n-1}} \tag{12}$$

According to the definition of the effective stress given in Eq. (7), $\dot{\bar{\sigma}}$ is derived as

$$\dot{\bar{\sigma}} = \frac{1}{\bar{\sigma}}\left\{\frac{3}{2}\sigma_{22}\dot{\sigma}_{22} + 3a_{66}\sigma_{12}\dot{\sigma}_{12}\right\} \tag{13}$$

By substituting Eq. (13) together with Eq. (9) into Eq. (6), the plastic shear strain rate $\dot{\gamma}_{12}^{\mathrm{p}}$ is obtained as

$$\dot{\gamma}_{12}^{\mathrm{p}} = \frac{9a_{66}^2\sigma_{12}^2}{H_{\mathrm{p}}\bar{\sigma}^2}\dot{\sigma}_{12} + \frac{9a_{66}\sigma_{12}\sigma_{22}}{2H_{\mathrm{p}}\bar{\sigma}^2}\dot{\sigma}_{22} \tag{14}$$

Substitution of Eq. (14) in Eq. (4) leads to the total shear strain rate

$$\dot{\gamma}_{12} = \dot{\gamma}_{12}^{\mathrm{e}} + \dot{\gamma}_{12}^{\mathrm{p}} = \left(\frac{1}{G_{12}^{\mathrm{e}}} + \frac{9a_{66}^2\sigma_{12}^2}{H_{\mathrm{p}}\bar{\sigma}^2}\right)\dot{\sigma}_{12} + \frac{9a_{66}\sigma_{12}\sigma_{22}}{2H_{\mathrm{p}}\bar{\sigma}^2}\dot{\sigma}_{22} \tag{15}$$

where G_{12}^{e} is the elastic shear modulus of the composite. For off-axis specimens with small off-axis angles, σ_{22} is small as compared with σ_{12} (see Eq. (17) for coordinate transformation of stresses) and, thus, the second term on the right side of Eq. (15) can be neglected with the result

$$G_{12}^{\mathrm{ep}} = \frac{\dot{\sigma}_{12}}{\dot{\gamma}_{12}} = \left[\frac{1}{G_{12}^{\mathrm{e}}} + \frac{9a_{66}^2\sigma_{12}^2}{H_{\mathrm{p}}\bar{\sigma}^2}\right]^{-1} \tag{16}$$

For the S2/8552 glass/epoxy composite, the orthotropy coefficient a_{66} in the plastic potential function and other parameters in the viscoplasticity model were determined following the procedure described by Tsai and Sun (2002). This procedure involves conducting compression tests on off-axis block specimens of various off-axis angles at three different nominal strain rates 0.0001, 0.01 and 1 s^{-1}. For each strain rate, stress–strain curves for different off-axis specimens are obtained. Using the one parameter plastic potential given by Eq. (5) and the associated effective stress and effective plastic strain, these off-axis curves can be collapsed into a single master curve for each strain rate by selecting an a_{66} value. These master curves can be expressed in a power law with a rate dependent amplitude as shown in Eq. (11). The elastic moduli and the numerical values of the parameters in the viscoplasticity model thus established are summarized in Table 1.

3.2. Dynamic microbuckling model for off-axis specimens

For off-axis composite specimens under compressive loading, the effective total fiber off-axis angle relative to the loading direction consists of the initial off-axis angle (θ), the initial fiber misalignment angle (ϕ) and the load-produced in-plane shear strain (γ_{12}). It is noted that during loading, the initial off-axis angle and initial fiber misalignment remain constant, but the in-plane shear strain is dependent on the applied load level. Thus, we define the effective off-axis angle ($\bar{\theta}$) as the sum of the initial off-axis angle (θ) and the initial fiber misalignment angle (ϕ).

Table 1
Elastic moduli and parameters for the viscoplasticity model for S2/8552 glass/epoxy

E_1	50 GPa
E_2	20 GPa
G_{12}	6.9 GPa
v_{12}	0.3
a_{66}	6.0
χ	5.31E−14 $(\mathrm{MPa})^{-n}$
m	−0.178
n	4

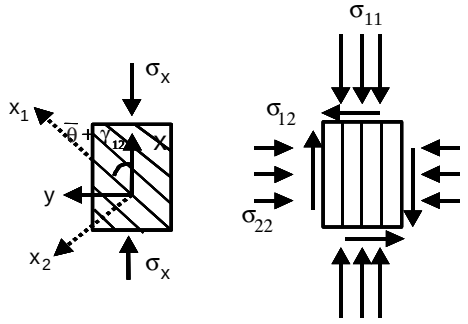

Fig. 3. Coordinate transformation for stresses in off-axis composite at the incipient of fiber microbuckling.

Using the coordinate transformation law, the uniaxial loading stress at the instant of fiber microbuckling can be decomposed into normal stresses and the in-plane shear stress in reference to the principal material directions as shown in Fig. 3. We have

$$\begin{aligned}\sigma_{11} &= \sigma_x \cos^2(\bar{\theta}+\gamma_{12}) \\ \sigma_{22} &= \sigma_x \sin^2(\bar{\theta}+\gamma_{12}) \\ \sigma_{12} &= -\sigma_x \sin(\bar{\theta}+\gamma_{12})\cos(\bar{\theta}+\gamma_{12})\end{aligned} \tag{17}$$

Based on the result of the bifurcation analysis given by Eq. (3), the compressive strength σ_{xc} for off-axis composites can be written as

$$\sigma_{xc}\cos^2(\bar{\theta}+\gamma_{12}) = G_{12}^{ep} \tag{18}$$

By substituting the stress components given by Eq. (17) in Eq. (16), the rate-dependent tangent shear modulus becomes

$$G_{12}^{ep} = \left[\frac{1}{G_{12}^{e}} + \frac{6a_{66}^2\cos^2(\bar{\theta}+\gamma_{12})}{H_p(\sin^2(\bar{\theta}+\gamma_{12}) + 2a_{66}\cos^2(\bar{\theta}+\gamma_{12}))}\right]^{-1} \tag{19}$$

Combining Eqs. (18) and (19), the microbuckling strength σ_{xc} for off-axis composites can be expressed explicitly in the form

$$\sigma_{xc}\cos^2(\bar{\theta}+\gamma_{12}) = \left[\frac{1}{G_{12}^{e}} + \frac{6a_{66}^2\cos^2(\bar{\theta}+\gamma_{12})}{H_p(\sin^2(\bar{\theta}+\gamma_{12}) + 2a_{66}\cos^2(\bar{\theta}+\gamma_{12}))}\right]^{-1} \tag{20}$$

It is noted that the induced in-plane shear strain is a function of the applied stress and strain rate. Moreover, the plastic modulus H_p in Eq. (20) is also nonlinearly related to the applied uniaxial stress σ_x. Thus, for a given effective off-axis angle $\bar{\theta}$ and strain history, a numerical iteration is employed to calculate the microbuckling stress σ_{xc} for off-axis composites. The uniaxial stress σ_x is increased incrementally from 0. At each stage, the effective stress $\bar{\sigma}$ and the plastic modulus H_p are updated using Eqs. (7) and (12), respectively. At the same time, the current in-plane shear strain is obtained by adding all the previous shear strain increments calculated using Eq. (15). This incremental procedure continues until Eq. (20) is satisfied. The applied stress at this step is the microbuckling stress σ_{xc}.

4. Compressive failure tests

In order to verify the dynamic microbuckling model, compressive failure tests were conducted on S2/8552 glass/epoxy composite specimens at various strain rates. Coupon specimens with end taps and anti-buckling fixtures are usually employed for quasi-static compression tests. However, in the high strain rate test using the SHPB, small block specimens were more suitable. In order to have consistency, block specimens were used for both low strain rate and high strain rate tests.

4.1. Low strain rate tests

For unidirectional composite specimens tested under end loading condition, fiber splitting was found to be the dominant failure mode. In order to prevent fiber splitting from happening ahead of fiber micro-buckling, off-axis block specimens were adopted for compressive failure tests. Off-axis block specimens of $0.6\times0.6\times1$ cm with fiber orientations of 5°, 10° and 15° (against the long direction), respectively, were cut from a 75-ply unidirectional S2/8552 glass/epoxy laminate using a diamond wheel. The specimens were lapped on a lapping machine with a 6 μm abrasive slurry to ensure smooth and flat loading surfaces. In addition, a lubricant was applied to the end surfaces of the specimen to reduce contact friction. A self-adjusting device as shown in Fig. 4 was used to eliminate potential bending moments and also to ensure the specimen to be in full contact with the loading surfaces. The applied load and displacement for each test were recorded using LabVIEW.

Off-axis specimens were tested in compression to failure using the stroke control mode on a servo-hydraulic MTS machine. Three different constant nominal strain rates of 10^{-4}, 10^{-2} and 1 s^{-1} were performed. The nominal strain rate was the stroke rate of the loading frame divided by the original specimen length. The corresponding true strain rates were measured by using strain gages directly mounted on the specimens. Fig. 5 shows the nominal strain curve and the true strain curve for a 15° specimen tested at the nominal strain rate of 0.0001 s^{-1}. It is evident that the true strain is quite different from the nominal strain and thus the true strain rate is also different from the nominal strain rate. The use of the self-adjusting device shown in Fig. 4 in the compression test could have contributed to this discrepancy. In this study, the true strain curve history was adopted for the calculation of the strain rate. Since the true strain rate is not constant during the loading process, the average value was employed in the analysis with the microbuckling model.

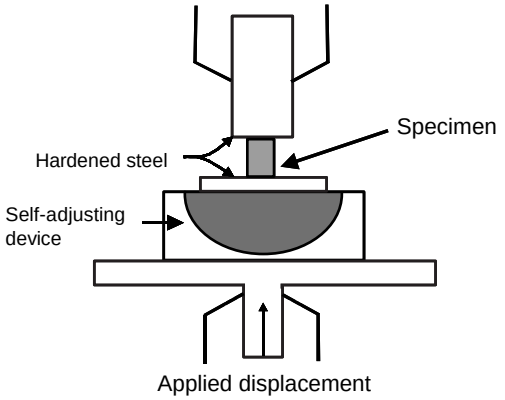

Fig. 4. Schematic of the compression test.

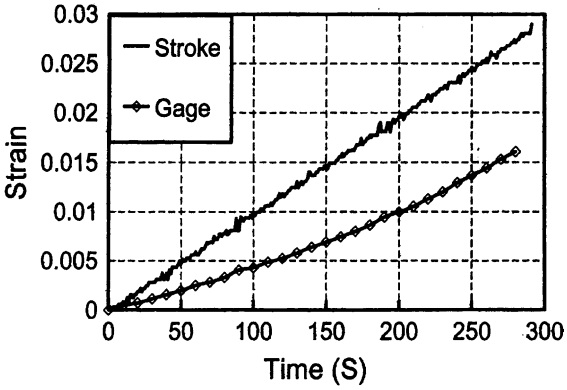

Fig. 5. Strain histories obtained from stroke and strain gage for 15° off-axis specimens tested at nominal strain rate 0.0001 s^{-1}.

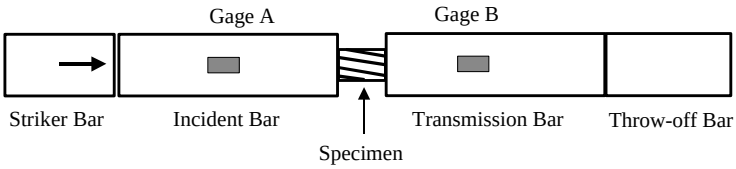

Fig. 6. Schematic of the split Hopkinson pressure bar for high strain rate compression test.

4.2. High strain rate tests

High strain rate compression tests were conducted using a split Hopkinson pressure bar (SHPB). Since the specimen is sandwiched between the incident bar and the transmission bar, shear-extension coupling occurs in the off-axis specimen under axial loading. This behavior combined with the bar-specimen interfacial contact friction could cause an inhomogeneous deformation in the specimen, which deviates from the conventional Hopkinson bar assumption. In order to reduce this contact friction, all specimens were lapped and lubricated as recommended by Ninan et al. (2001). A two-gage configuration of a split Hopkinson

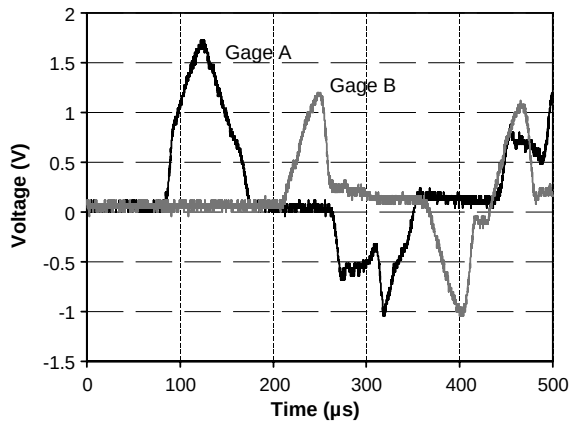

Fig. 7. Strain gage signals recorded in SHPB test for 10° off-axis specimen.

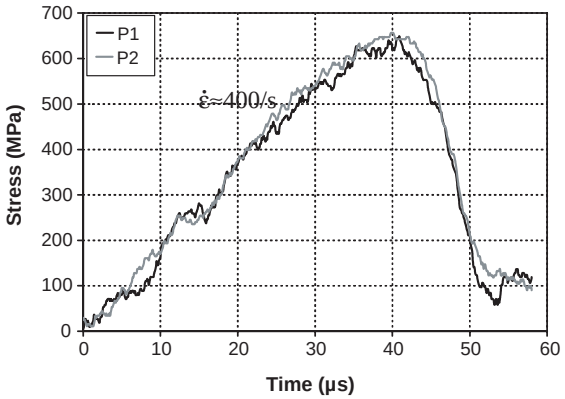

Fig. 8. Time histories of contact stresses for 10° off-axis specimen.

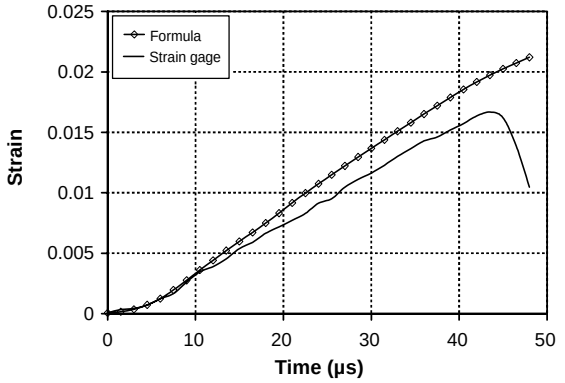

Fig. 9. Strain histories obtained from Hopkinson bar formula and strain gages, respectively, for a 10° off-axis specimen in SHPB test.

pressure bar is shown in Fig. 6, where gage A measures both the incident and reflected pulses in the incident bar, while gage B measures the transmitted pulse. Fig. 7 shows the typical signatures (voltages) picked up by strain gages A and B during an SHPB test on the 10° specimen. Using the Hopkinson bar theory, the contact stress P_1 between the incident bar and the specimen, and P_2, the contact stress between the specimen and the transmission bar, can be extracted from the recorded pulse data (Graff, 1975). Fig. 8 shows contact stresses P_1 and P_2 for the 10° specimen in the SHPB test. It can be seen that the peak values of the P_1 and P_2 curves are nearly the same. The average of the peak values was taken as the failure stress of the specimen in the SHPB test.

Conventionally, the strain history of the specimen during loading is calculated using a well known Hopkinson bar formula with expressions of displacements at the ends of the bars derived from the strain responses recorded at gages A and B (Graff, 1975). In the present study, the strain response of the specimen was also measured using strain gages directly mounted on the specimen. Fig. 9 shows the comparison of the strain histories for the 10° specimen obtained using the Hopkinson bar formula and the strain gage on the specimen, respectively. It is evident that the strain history calculated based on the Hopkinson bar theory deviates from that directly measured on the specimen. Consequently, the respective strain rates obtained were also different. In this study, the strain rate measured directly from the specimen was used. The average strain rates for the 5° specimen and 10 ° specimen were about 900 and 400 s^{-1}, respectively.

5. Model prediction

In the failure prediction analysis using the microbuckling model, Eq. (20) must be solved numerically. Specifically, the elastic–plastic modulus H_p and in-plane shear strain γ_{12} histories during loading are needed in Eq. (20). Theoretically, these quantities can be calculated from the measured load history using the viscoplasticity model with incremental procedures. In this study, we employed a simpler but approximate procedure based in part on the measured strain history of the specimen. As indicated in Fig. 5, the actual strain rate in the specimen was not the same as the nominal strain rate and was not constant during loading. In this study, the strain measured with strain gages was used, from which the plastic strain was extracted by subtracting from it the elastic strain. The state of stress in off-axis composite specimens under uniaxial loading is in a state of proportional loading and, thus, the effective plastic strain rate $\dot{\bar{\varepsilon}}^p$ is related to the loading plastic strain rate as (Thiruppukuzhi and Sun, 2001).

$$\dot{\bar{\varepsilon}}^p = \frac{\dot{\varepsilon}_x^p}{h(\bar{\theta})} \tag{21}$$

where

$$h(\bar{\theta}) = \sqrt{\tfrac{3}{2}}\left[\sin^4\bar{\theta} + 2a_{66}\sin^2\bar{\theta}\cos^2\bar{\theta}\right]^{1/2} \tag{22}$$

Theoretically, the induced shear strain should be added to the off-axis angle term $\bar{\theta}$ in Eq. (21). In view of the fact that a variation in plastic strain rate does not affect the strength unless it is more than an order of magnitude, only the fiber off-axis angle and misalignment angle are included in $\bar{\theta}$. Moreover, to further simplify the calculation, the average plastic strain rate for each test is used in calculating the plastic modulus H_p using Eq. (12). Table 2 lists the average strain rates based on the strain histories measured with strain gages. For each off-axis specimen, the plastic strain history is obtained by subtracting the elastic strain from the total strain response history. Subsequently, the plastic strain rate history and the average plastic strain rate are obtained. The corresponding average effective plastic strain rate is obtained using Eq. (21).

Once the average effective plastic strain rate is adopted, the evaluation of Eq. (20) only requires the input of the value of γ_{12} corresponding to the axial loading stress σ_x. The incremental solution procedure is performed starting with $\sigma_x = 0.0$. The shear strain increment for each load increment can be calculated from Eq. (15) in which H_p is determined with the average effective plastic strain rate, and the stress components are obtained from the stress transformation law given by Eq. (17) in which γ_{12} is the value of the previous step. The compressive strength σ_{xc} is obtained when Eq. (20) is satisfied.

6. Experimental results and comparison

All failed specimens from compression tests were examined using a microscope to observe the failure mechanism. For 5° and 10° specimens, fiber microbuckling was found to be the dominant failure mecha-

Table 2
The average stain rate and the corresponding nominal strain rate in compressive failure tests

Low strain rate test	Average strain rate
Nominal strain rate 1.0E−4 s^{-1}	5.2E−5 s^{-1}
Nominal strain rate 1.0E−2 s^{-1}	4.2E−3 s^{-1}
Nominal strain rate 1 s^{-1}	0.25 s^{-1}
High strain rate test	Average strain rate
Strain rate from formula 500 s^{-1}	400 s^{-1}
Strain rate from formula 1000 s^{-1}	900 s^{-1}

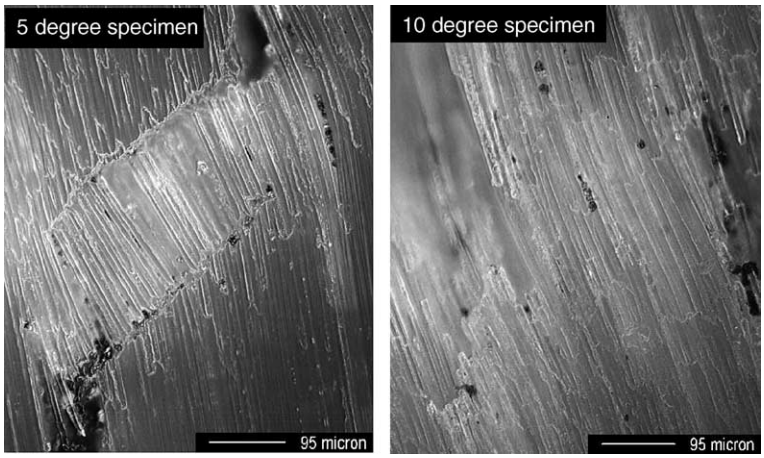

Fig. 10. Microbuckling failure mechanism in 5° and 10° off-axis specimens.

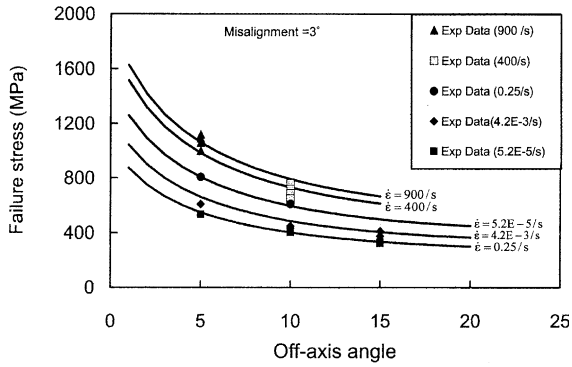

Fig. 11. Comparison of experimental and predicted microbuckling failure strengths for 5°, 10° and 15° S2/8552 off-axis specimens.

nism within the range of tested strain rates. For the 15° specimen, failure was dominated by fiber microbuckling at strain rates below 0.01 s^{-1}; and was dominated by matrix shear failure at higher strain rates. This phenomenon indicates that the fiber microbuckling load and shear failure load in the 15° specimen must be very close. At lower strain rates the shear stiffness is lower than that at high strain rates. Fig. 10 shows the failure mechanism of fiber microbuckling in the 5° and 10° off-axis specimens tested at the nominal strain rate of 10^{-4} s^{-1}.

In a recent study by Tsai and Sun (2003), it was found that the 30° and 45° S2/8552 off-axis specimens all failed in in-plane shear mode for both low and high strain rates. This result is expected because for these large off-axis angles, the in-plane shear stress component induced by axial compression is significant relative to the shear strength of the composite, making it possible for shear failure to take place before fiber microbuckling.

The experimental failure stresses σ_{xc} for off-axis specimens at different strain rates are shown in Fig. 11. Only the data associated with microbuckling are included in the figure. The model predictions with a 3° initial fiber misalignment are also presented in the figure for comparison. The 3° initial fiber misalignment was chosen to fit the experimental data. This value is within the experimental measurements of fiber misalignment of composites (Yurgartis, 1987). It is evident that the microbuckling stress is significantly

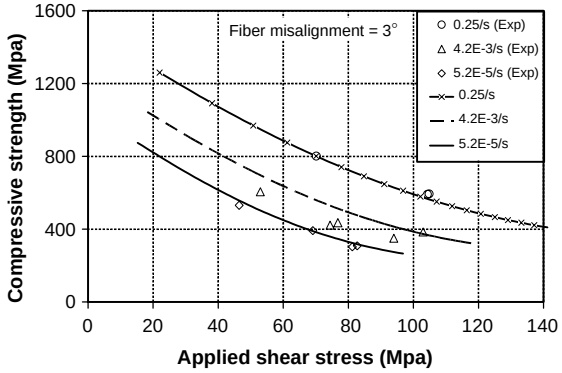

Fig. 12. Critical compressive axial stresses versus shear stress for S2/8552 glass/epoxy composite for three different strain rates. The lines indicate model predictions for different strain rates.

affected by strain rate. Comparison of model predictions with the test data indicates that the present dynamic microbuckling model is capable of predicting the compressive failure stress of the composite for strain rates (up to 900 s^{-1}) considered in this study.

7. Effect of shear stress

Owing to the extension-shear coupling in off-axis composite specimens, fiber microbuckling in these specimens takes place in the presence of shear stresses. Thus, the effect of shear stress on compressive strength in fiber composites can be assessed from the compression data for the off-axis composite specimens. Specifically, the critical axial stress σ_{11c} (the compressive longitudinal strength of the composite) and the corresponding shear stress σ_{12} were obtained from the failure stress σ_{xc} for off-axis specimens with the aid of Eq. (17). These stress components are the apparent stresses without considering the fiber misalignment and shear strain effect. For this purpose, only the initial off-axis angle was considered in the coordinate transformation using Eq. (17).

Fig. 12 shows the experimental results and model predictions (with a 3° initial fiber misalignment) of compressive strength versus in-plane shear stress σ_{12} for different strain rates. The model predictions are also included for comparison. It is clear that the presence of shear stress can greatly alter the longitudinal compressive strength of the composite. More specifically, the compressive strength of the composite decreases as the in-plane shear stress increases. This effect can be attributed to the fact the presence of the in-plane shear stress can reduce the value of the elastic–plastic shear modulus. Thus, the compressive strength of a composite subjected to combined compression and shear loads must be evaluated by taking into account the effect of shear stress. A similar result was observed by Jelf and Fleck (1994) who performed torsion–compression tests on unidirectional composite tubes.

8. Comparison of microbuckling model and kink band model

There are two major models developed for prediction of compressive strengths of polymeric composites, namely, the microbuckling model and the kink band model. The two models were derived based on different assumptions and have different functional forms for the compressive longitudinal strength (Sun and Tsai, 2001). In this section, a comparison of the two models is presented. Table 3 shows the compressive

Table 3
Comparison of compressive strengths of S2/8552 off-axis specimens predicted using microbuckling model and kink band model

Off-axis angle	5°	10°
Experimental data (MPa)	535	404
Kink band model (MPa)	554	395
Microbuckling model (MPa)	550	403

failure predictions for 5° and 10° off-axis S2/8552 glass/epoxy composite specimens at a nominal strain rate of 10^{-4} s^{-1} using the present microbuckling model with a 3° initial fiber misalignment and the kink band model by Budiansky and Fleck (1993) with a 2° initial fiber misalignment. The comparison indicates that the compressive strengths for the off-axis specimens obtained from the two models are basically the same and agree with the experimental data well.

It is noted that in the kink band model by Budiansky and Fleck (1993), only the shear stress component is taken into account and the effect of other stress components are neglected. This is acceptable for off-axis specimens with small off-axis angles in which the transverse normal stress σ_{22} is small. Slaughter et al. (1993) extended the kink band model to include the combined stress effect on plasticity. By considering the continuity of tractions and displacement on the boundary of the band and assuming a homogeneous deformation inside and outside the kind band, implicit equations for compressive strength were derived. For strain hardening composite materials with a nonzero kink band angle β, the functional form for compressive strength is quite complicated. It appears that the kink band model is more cumbersome to use than the microbuckling model in predicting compressive failure of composites under a general state of stress.

9. Conclusions

In this study, it has been shown that, by including fiber misalignments and matrix nonlinear behavior, the microbuckling model can be extended to predict compressive strengths of polymeric composites under low and high strain rate loadings. The viscoplasticity model developed by Tsai and Sun (2002) for composites can be incorporated in the microbuckling model to account for the strain rate effect on compressive strength. Experimental results from off-axis compression tests on the S2/8552 glass/epoxy composite indicate that fiber microbuckling failure mode and, thus, the compressive longitudinal strength of the composite can be obtained from off-axis specimens with small (5–15°) off-axis angles. From model predictions as well as experimental results it is concluded that the compressive strength of polymeric composites is rate-sensitive and that the presence of in-plane shear stress can appreciably lower the compressive longitudinal strength.

It is also concluded that, although the initial concepts of the two models are different, the microbuckling model and the kink band model predict basically the same compressive strength of off-axis composite specimens with small off-axis angles.

Acknowledgement

This work was supported by an Office of Naval Research Grant No. N00014-96-0822.

References

Argon, A.S., 1972. Fracture of composites. In: Treatise on Materials Science and Technology, vol. 1. Academic Press, NY, pp. 79–114.
Budiansky, B., 1983. Micromechanics. Computer and Structures 16 (1), 3–12.

Budiansky, B., Fleck, N.A., 1993. Compressive failure of fiber composites. Journal of Mechanics and Physics of Solids 41 (1), 183–221.
El-Habak, A.M.A., 1993. Compressive resistance of unidirectional GFRP under high rate of loading. Journal of Composites Technology & Research 15 (4), 311–317.
Graff, K.F., 1975. Wave Motion in Elastic Solids. Dover Publications, New York.
Jelf, P.M., Fleck, N.A., 1994. The failure of composite tubes due to combined compression and torsion. Journal of Materials Science 29 (11), 3080–3084.
Kumar, P., Garg, A., Agarwal, B.D., 1986. Dynamic compressive behavior of unidirectional GFRP for various fiber orientations. Materials Letters 4 (2), 111–116.
Lankford, J., 1991. Compressive damage and fatigue at high loading rates in graphite fiber-reinforced polymeric matrix composites. Ceramic Transactions 19, 553–563.
Ninan, L., Tsai, J., Sun, C.T., 2001. Use of split Hopkinson pressure bar for testing off-axis composites. International Journal of Impact Engineering 25, 291–313.
Rosen, B.W., 1965. Mechanics of composite strengthening. In: Fiber Composites Materials. American Society of Metals, Metals Park, OH, pp. 35–75.
Slaughter, W.S., Fleck, N.A., Budiansky, B., 1993. Compressive failure of fiber composites: the roles of multiaxial loading and creep. Journal of Engineering Materials and Technology 115 (3), 308–313.
Sun, C.T., Chen, J.L., 1989. A simple flow rule for characterizing nonlinear behavior of fiber composites. Journal of Composite Materials 23 (10), 1009–1020.
Sun, C.T., Jun, A.W., 1994. Compressive strength of unidirectional fiber composites with matrix non-linearity. Composites Science and Technology 52 (4), 577–587.
Sun, C.T., Tsai, J.L., 2001. Comparison of microbuckling model and kink band model in predicting compressive strength of composites. In: Proceedings of the 13th International Conference on Composite Materials, Beijing, China.
Thiruppukuzhi, S.V., Sun, C.T., 2001. Models for strain rate-dependent behavior of polymer composites. Composites Science and Technology 61 (2001), 1–12.
Tsai, J., Sun, C.T., 2002. Constitutive model for high strain rate response of polymeric composites. Composite Science and Technology 62 (10–11), 1289–1297.
Tsai, J., Sun, C.T., 2003. Strain rate effect on in-plane shear strength of unidirectional polymeric composites. In: ICCM 14, 2003. Proceedings of 14th International Conference on Composite materials (ICCM 14), San Diego, July, pp. 14–18.
Yuan, J., Takeda, N., Waas, A.M., 1999. Comparison of impact compressive failure of GFRP and CFRP unidirectional composites. In: Shim, V.P.W., Tanimura, S., Lim, C.T. (Eds.), Impact Response of Materials and Structures. 3rd International Symposium on Impact Engineering. Oxford University Press, Oxford, pp. 184–189.
Yurgartis, S.W., 1987. Measurement of small angle fiber misalignments in continuous fiber composites. Composite Science and Technology 30 (4), 279–293.